AIP | Applied Physics Letters

Underwater microwave ignition of hydrophobic thermite powder enabled by the bubble-marble effect

Yehuda Meir and Eli Jerby

Citation: Applied Physics Letters **107**, 054101 (2015); doi: 10.1063/1.4928110
View online: http://dx.doi.org/10.1063/1.4928110
View Table of Contents: http://scitation.aip.org/content/aip/journal/apl/107/5?ver=pdfcov
Published by the AIP Publishing

Underwater microwave ignition of hydrophobic thermite powder enabled by the bubble-marble effect

Yehuda Meir and Eli Jerby[a)]
Faculty of Engineering, Tel Aviv University, Ramat Aviv 6997801, Israel

(Received 8 July 2015; accepted 25 July 2015; published online 4 August 2015)

Highly energetic thermite reactions could be useful for a variety of combustion and material-processing applications, but their usability is yet limited by their hard ignition conditions. Furthermore, in virtue of their zero-oxygen balance, exothermic thermite reactions may also occur underwater. However, this feature is also hard to utilize because of the hydrophobic properties of the thermite powder, and its tendency to agglomerate on the water surface rather than to sink into the water. The recently discovered *bubble-marble* (BM) effect enables the insertion and confinement of a thermite-powder batch into water by a magnetic field. Here, we present a phenomenon of underwater ignition of a thermite-BM by localized microwaves. The thermite combustion underwater is observed *in-situ*, and its microwave absorption and optical spectral emission are detected. The vapour pressure generated by the thermite reaction is measured and compared to theory. The combustion products are examined *ex-situ* by X-ray photo-electron spectroscopy which verifies the thermite reaction. Potential applications of this underwater combustion effect are considered, e.g., for detonation, wet welding, thermal drilling, material processing, thrust generation, and composite-material production, also for other oxygen-free environments. © *2015 AIP Publishing LLC*. [http://dx.doi.org/10.1063/1.4928110]

Thermite reactions between metals and metal-oxides tend to burn at relatively high temperatures, but they require high temperatures as well for ignition.[1,2] For example, the self-propagating reaction of a mixed magnetite and aluminium powder produces iron and alumina in the reduction process,

$$3Fe_3O_4 + 8Al \rightarrow 9Fe + 4Al_2O_3 + 3.67\,kJ/g, \qquad (1)$$

in a flame with a theoretical adiabatic temperature of 4057 K,[2,3] which requires an ignition temperature of ~1500 K.[4] Thermite reactions are used for various applications, including welding, self-propagating high-temperature syntheses (SHS), and combustion syntheses (CS).[4–6] The porous ceramic-metal materials obtained in relatively low-cost rapid processes are characterized by superior micro-structural and mechanical properties.[7]

The thermite reaction is featured by an inherent zero-oxygen balance (note the oxygen exchange in Eq. (1) from the iron oxide to the aluminium in a diffusive burning). Therefore, thermite can also react in oxygen-free environments (such as in vacuum) or underwater where oxygen barely exists before combustion. Gasses are exhausted from the combusted thermite-powder by heating the surrounding medium (e.g., air) rather than directly from the interaction itself. The gas emission can be enhanced by using carbon or boron nanoparticles as additives, in order to produce CO, CO_2, or B_2O_3.[8,9] Thermite is considered as a green-energy heating source since it does not emit CO, NO_x, or SO_x gasses, or heavy metals.[10]

Fine thermite powders (with particle size in the micrometer range or smaller) are characterized as hydrophobic powders, hence they hardly penetrate into water. To overcome this difficulty, thermite powders are sometimes solidified and coated in order to enable their insertion into water.[11,12] The packed powder is then heated up to its ignition temperature inside the water. The recently discovered bubble-marble (BM) effect[13] utilizes the hydrophobicity of the aluminium in a fine thermite mixture in order to encapsulate the powder in a bubble form, which sinks into water by the influence of an external magnetic field.

Microwave energy applied for combustion synthesis improves the reaction process and its products due to the microwave volumetric heating.[14] On the other hand, the localized microwave heating (LMH) effect enables rapid heating by intentionally induced thermal-runaway instability within a confined hotspot.[15,16] The ignition of a pure thermite powder by LMH was recently demonstrated in ambient air.[17] This finding leads to the development of efficient LMH igniters for thermites.[18] The combined BM and LMH effects enable the underwater ignition of thermite powder, as demonstrated and investigated in this study.

The underwater LMH-ignition mechanism of pure thermite powder is illustrated in Fig. 1. The Fe_3O_4-Al thermite mixture is a hydrophobic powder with ferrimagnetic features attributed to its magnetite component. Thus, the powder tends to reside on the water-air interface in order to minimize its surface-tension free energy (which dominates over gravity). By inducing a magnetic-field gradient parallel to gravity, the thermite powder is agglomerated into a bubble shape by the capillary force, and sinks in a BM form towards the underwater magnetic pole.[13] Once stabilized, the BM is irradiated by microwaves. In the LMH process evolved, the thermal-runaway instability raises the local temperature up to the thermite ignition point (as in Ref. 16) thus initiating combustion within the encapsulated thermite-BM. The

[a)]Author to whom correspondence should be addressed. Electronic mail: jerby@eng.tau.ac.il

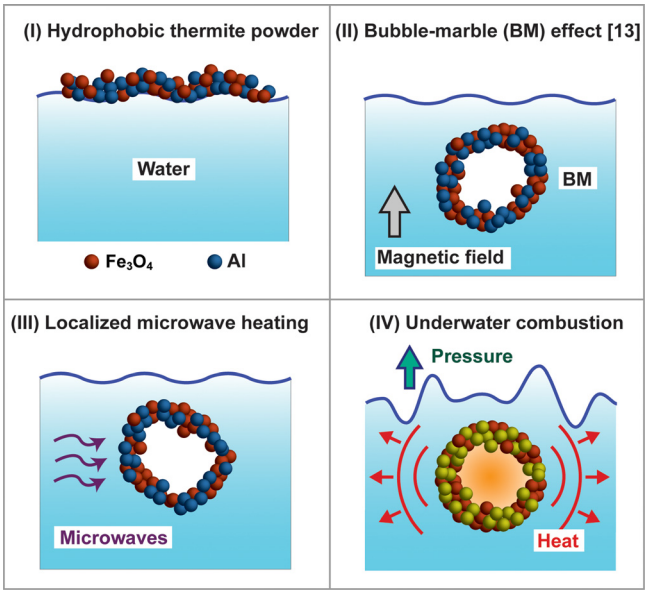

FIG. 1. A conceptual illustration of the underwater thermite ignition enabled by the bubble-marble (BM) effect in the following stages: (I) The thermite powder initially resides on the water-air interface. (II) The applied magnetic field attracts the thermite into the water, and forms a BM. (III) The BM is irradiated underwater by localized microwaves and (IV) its consequent ignition leads to self-propagating combustion of the thermite batch.

generated heat melts the powder along the combustion front (as in an ordinary thermite welding process in air). The heat exhausted by the thermite combustion underwater is transferred to the surrounding water, hence locally boiling the water. The excess vapor emission generates then a burst of relatively high pressure.

The experimental setup illustrated in Fig. 2 consists of a microwave cavity fed by a magnetron tube (2.45-GHz, 1 kW, pulsed at 50 Hz) via a microwave reflectometer, which enables amplitude and phase measurements of the incident and reflected waves. The thermite mixture used is composed of 76% magnetite (Iron Black 318) and 24% aluminum (Al-400)

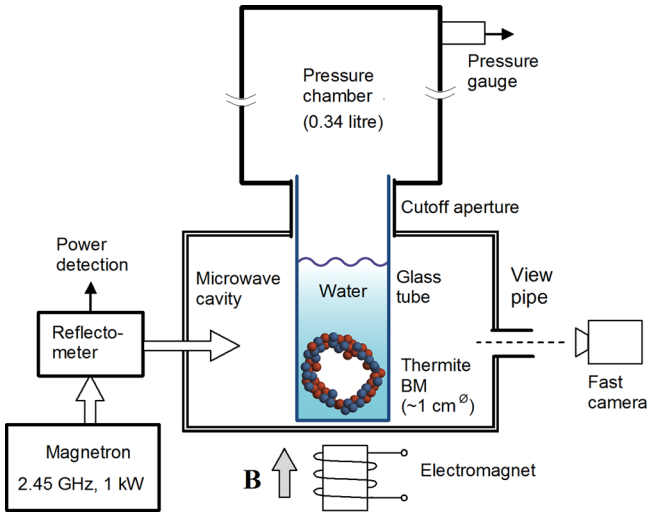

FIG. 2. The experimental setup employed in this study consists of a microwave cavity fed by a 2.45-GHz magnetron via a reflectometer. The thermite powder in the water tube is attracted by the magnetic-field gradient applied by the electromagnet underneath, and forms a BM inside the water. The vapors generated by the thermite combustion are accumulated in the pressure chamber and measured by a pressure gauge.

powders, with ~45-μm and ~37-μm particle diameters, respectively. The thermite batch is poured to a cylindrical glass tube (18-mm$^{\varnothing}$) filled with 7-cm^3 tap water. An electromagnet placed underneath generates a 0.03-T magnetic-flux density perpendicular to its pole. The ~0.1 T/m gradient induced in the glass tube is sufficient to form a BM from a batch of ~0.1–g thermite. The vapors generated by the thermite combustion are accumulated above, in a 0.34-l pressure chamber. A pressure transducer (ELCON 30.600G) enables measurements of isometric pressure versus time in the range of 0–2.5 bar. An optical spectrometer (Avantes Avaspec-3648) in the 200–1000 nm wavelength range (0.3-nm spectral resolution) is used to capture the light emitted from the underwater combustion. The measured intensity is calibrated by an AvaLight Deuterium-Halogen light source (DH-BAL-CAL UV/VIS). A high-speed camera (300 frames/s, SV-643C) is used to record the process. The solid products of the combustion are tested by X-ray photoelectron spectroscopy (XPS) in a 2.5×10^{-10} Torr base pressure using an Al K_α monochromated source (1486.6 eV with sputtering rate capabilities of ~31.5 Å/min by 4 kV Ar^+ ion gun). The product conductivity is measured by an ohmmeter (DT830D), and its volume is estimated by Archimedes' law in ethanol.

A typical ignition process is shown in Figs. 3(a) and 3(b). The microwave power absorbed by the water and

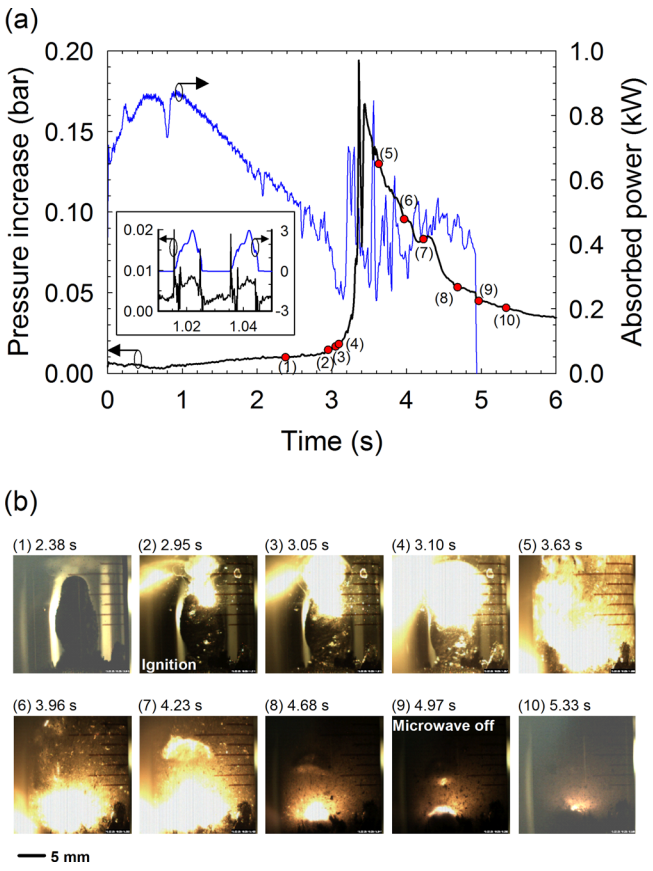

FIG. 3. A typical localized-microwave ignition process of a thermite-BM in water. (a) The microwave power absorbed by the thermite-BM in water, and the consequent pressure increase in the chamber. The inset shows the detection sensitivity by the fine pressure response (prior to ignition) to the 50-Hz pulsation of the microwave power. (b) Sequential images recorded during the microwave irradiation process (in times marked by red circles in Fig. 3(a)), which show the underwater ignition and combustion of the thermite-BM.

thermite-BM up to ignition and the generated pressure evolved in the chamber during this isometric process are presented in Fig. 3(a). The ignition occurs after 2.95 s of microwave radiation, as seen in the sequential images in Fig. 3(b). The total microwave energy absorbed in water during this period prior to ignition is 2.2 kJ. The hotspot evolved within the BM ignites the thermite batch, which erupts as a mushroom-like flame within the water. An abrupt increase in the chamber pressure is recorded soon after ignition, and the microwave absorption becomes erratic. The thermite combustion lasts ~2 s, and the microwave power is turned off afterwards. The water boiling due to combustion is seen by the ejected fire bubbles in Fig. 3(b). Additional smaller BMs are ejected from the combusted thermite towards the glass walls. The combustion product (~0.06 g in weight) is collected after the process for *ex-situ* analyses.

The sensitivity of the measurements presented in Fig. 3(a) is demonstrated in the inset, which shows the fine response of the microwave and pressure detectors (prior to ignition) to the 50-Hz pulsation of the magnetron. This inherent modulation of the microwave heating also enables a distinction between the relatively slow heating of the water by the microwaves, and their rapid evaporation due to the thermite combustion (note that the microwave energy supplied is insufficient to boil the water directly).

The optical spectrum of the thermite combustion, shown in Fig. 4, is detected from above the water tank (with the pressure chamber removed); hence, the emitted light is transferred through the water and therefore attenuated. The optical spectrum exhibits a continuum radiation, which using Plank's law fits to a blackbody temperature of ~2100 K (dashed line). This temperature is lower than the ideal adiabatic thermite flame temperature due to water quenching. Iron and aluminum spectral lines are shown in the inset, as captured in the near ultraviolet (UV) region at the beginning of the combustion process (before being masked by the continuum radiation of the blackbody emission with the higher intensity). Similar spectral lines were observed in thermite ignition by microwaves in air.[17]

The dependence of the pressure generated on the combusted thermite mass is shown in Fig. 5. A nearly linear

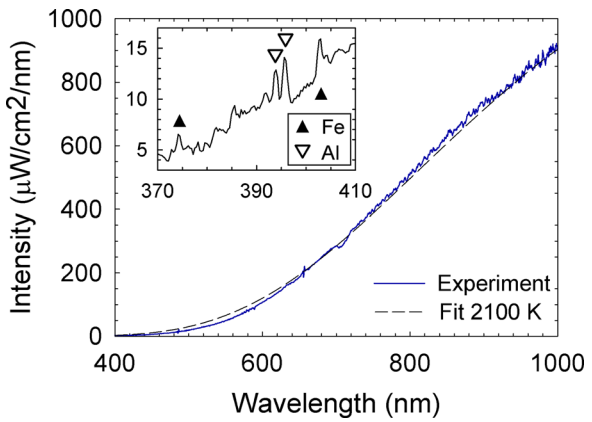

FIG. 4. The optical emission spectrum observed from the combusted thermite-BM underwater, and the temperature fitting to 2100 K estimated by blackbody radiation. The inset shows the iron (Fe) and aluminium (Al) spectral lines in the near UV region (captured at the beginning of the combustion process).

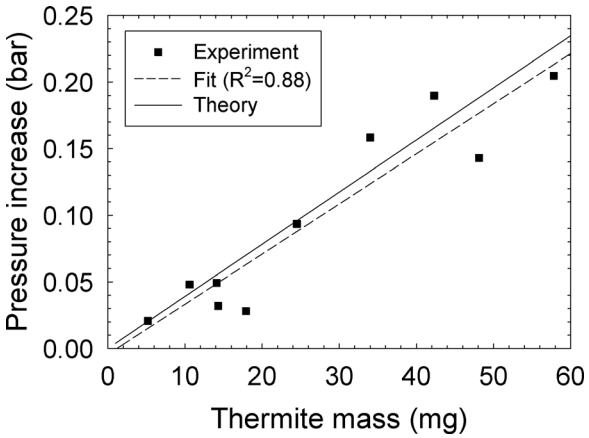

FIG. 5. The pressure variation in the chamber during combustion vs. the thermite-BM mass. The graph shows the experimental results and their linear fit in a comparison to the theoretical energy-conservation estimate presented in Eq. (2).

dependence of the measured pressure increase on the thermite mass is observed in the range of 6–58 mg. A linear fit of the experimental results (dashed line) is compared in Fig. 5 to a theoretical estimate of the pressure generated (solid line). The latter is given by

$$\frac{\Delta P}{\Delta m_{Th}} \cong \frac{E_{Th}}{L_V \rho_a} \frac{P_{amb}}{V_{Ch}}, \tag{2}$$

where ΔP is the pressure variation in the chamber, Δm_{Th} is the burned thermite mass, $E_{Th} = 3.67\text{kJ/g}$ is the thermite's stored energy, $L_V = 2.26\text{kJ/g}$ is the water latent heat, $\rho_a = 1.2\,\text{g/l}$ is the air density at atmospheric pressure, $P_{amb} = 1\,\text{bar}$ is the ambient atmospheric pressure, and $V_{Ch} = 0.34\,\text{l}$ is the volume of the pressure chamber. Equation (2) is derived from the ideal gas law, reduced in this isometric case to $\Delta P/\Delta m_W \cong P_{amb}/m_a$, where Δm_W is the mass of the evaporated water and $m_a = \rho_a V_{Ch}$ is the mass of the air stored in the pressure chamber. Assuming that the energy emitted by the thermite combustion ($E_{Th}\Delta m_{Th}$) is absorbed entirely by the water latent heat ($L_V \Delta m_W$) due to the high temperature evolved, the approximated mass of the evaporated water is $\Delta m_W \cong E_{Th}\Delta m_{Th}/L_V$, which leads to Eq. (2). Figure 5 shows an agreement of $R^2 = 0.88$ between this linear model and the experimental results.

The underwater combustion of thermite-BM produces a solid ceramic-metal sphere, as shown, for instance, by the bubble-like hollow sphere (0.17-g in weight) in the inset of Fig. 6. An XPS analysis performed on the outer surface of the combusted sphere (after removing a 0.1-μm thick layer by sputtering for 30 min) reveals peaks of iron, aluminum, and oxygen, as shown in Fig. 6. A higher resolution analysis (0.05 eV/step) reveals their chemical bonding, in which part of the iron is pure and most of the aluminum is oxidized, as evident by the peak divergence. The results confirm the reduction of the initial magnetite and aluminum to iron and alumina, according to Eq. (1). The color of the sphere shown in the inset is typical to the iron-alumina ceramic generated, with some small rusty spots inside. The shell density of this hollow sphere is ~2.7 g/cm^3 (lower than of iron and aluminum), and its electrical resistivity is ~1 kΩ (both indicate its

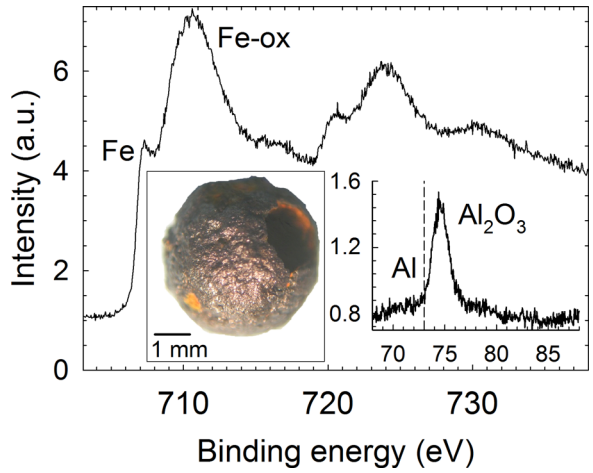

FIG. 6. An XPS analysis of the thermite combustion product. The alumina-iron matrix detected is an evidence for the thermite reduction process described in Eq. (1). The inset shows an example of a hollow sphere produced by the thermite-BM combustion.

porous structure). The combustion product also exhibits some magnetic properties (e.g., by its considerable attraction to permanent magnets).

The energy released by 0.1-g thermite combustion is 0.367 kJ (1). Compared to the 2.2-kJ microwave energy delivered to the entire water volume in this experiment, the added energy obtained is ~17%. However, since only ~2% of the water was evaporated, in the vicinity of the thermite BM, one may expect that improving the microwave guiding and localization in this region (e.g., by an LMH applicator[17]) would significantly increase the relative added energy (towards the 20× factor demonstrated in air[17]).

This study shows that hydrophobic pure-thermite powder can be effectively ignited by LMH, after its encapsulation underwater as a BM by magnetic field. The consequent combustion is detected by measuring the temperature and pressure generated, and by visual observation. The combustion solid product is analyzed, also in order to verify the thermite reaction (1). The pressure increase due to the rapid boiling of the water surrounding the combusted thermite-BM is found in agreement with an energy-conservation estimate (2).

The underwater microwave ignition process can be further elaborated in future studies. For instance, the LMH effect (induced remotely here with no physical contact) can be enhanced by a closer proximity of the applicator to the thermite-BM (as, for instance, in the LMH electrode scheme demonstrated in air[17]). The thermite BM can also be pre-encapsulated in water and frozen into an ice cube in advance, hence alleviating the need for applying a magnetic field while underwater ignition.

The underwater combustion effect presented here may open possibilities for advanced applications in oxygen-free environments, such as outer space, or underwater, where oxygen barely exists before the combustion. These include material-processing applications, such as CS of hard materials[18] and composite materials, ceramics production from iron oxides (e.g., as existed on Mars or moon) in vacuum conditions,[19] and fabrication of solids with magnetic properties (such as cermet-based porous ceramics). For nano-powder explosives,[8] the usage of thermites for explosion and detonation can also be extended to underwater scenarios. The heat released by the thermite reaction can also be utilized for underwater construction works such as wet welding[20] and thermal drilling. Thermite combustion can also be used to produce thrust, e.g., for underwater propulsion using the combined BM and LMH effects.

This study was supported by the Israel Science Foundation (ISF) Grant No. 1639/11.

Dr. Larisa Burstein is acknowledged for the XPS analyses.

[1]L. L. Wang, Z. A. Munir, and Y. M. Maximov, J. Mater. Sci. **28**, 3693 (1993).
[2]L. Duraes, J. Campos, and A. Portugal, Propellants Explos. Pyrotech. **31**, 42 (2006).
[3]S. H. Fischer and M. C. Grubelich, in Proceedings of the 24th Int'l Pyrotechnics Seminar, Monterey, CA, 1998.
[4]C. C. Lee, N. Yoshikawa, and S. Taniguchi, J. Mater. Sci. **46**, 7004 (2011).
[5]T. Lu and Y. Pan, J. Mater. Sci. **45**, 5923 (2010).
[6]T. Lu and Y. Pan, Mater. Manuf. Processes **27**, 914 (2012).
[7]G. Liu, J. Li, and K. Chen, Int. J. Refract. Met. Hard Mater. **39**, 90 (2013).
[8]K. S. Martirosyan, J. Mater. Chem. **21**, 9400 (2011).
[9]K. S. Martirosyan, L. Wang, A. Vicent, and D. Luss, Propellants Explos. Pyrotech. **34**, 532 (2009).
[10]S. Georg and T. M. Klapötke, Angew. Chem. Int. Ed. **47**, 3330 (2008).
[11]E. Nixon, M. L. Pantoya, G. Sivakumar, A. Vijayasai, and T. Dallas, Surf. Coat. Technol. **205**, 5103 (2011).
[12]S. C. Stacy, M. L. Pantoya, D. J. Prentice, E. D. Stejfler, and M. A. Daniels, Adv. Mater. Process. **167**, 33 (2009).
[13]Y. Meir and E. Jerby, Phys. Rev. E **90**, 030301 (2014).
[14]R. Rosa, P. Veronesi, and C. Leonelli, Chem. Eng. Process. **71**, 2 (2013).
[15]E. Jerby, V. Dikhtyar, O. Aktushev, and U. Grosglick, Science **298**, 587 (2002).
[16]E. Jerby, O. Aktushev, and V. Dikhtyar, J. Appl. Phys. **97**, 034909 (2005).
[17]Y. Meir and E. Jerby, Combust. Flame **159**, 2474 (2012).
[18]Y. Meir and E. Jerby, U.S. patent application WO 2012120412 A1 (13 September 2012).
[19]G. Corrias, R. Licheri, R. Orru, and G. Cao, Acta Astronaut. **70**, 69 (2012).
[20]J. Labanowski, D. Fydrych, and G. Rogalski, Adv. Mater. Sci. **8**, 11 (2008).